

Diagrammatic Design of Ansätze for Quantum Chemistry



Ayman El Amrani

St. John's College

A thesis submitted for the Honour School of Chemistry

Part II 2024

Pour ma mère et mon père.

Summary

A central challenge in computational quantum chemistry is the accurate simulation of fermionic systems. At the heart of these calculations lies the need to solve the Schrödinger equation to determine the many-electron wavefunction. An exact solution to this problem scales exponentially with the number of electrons. Classical computers have no means by which to efficiently store the increasingly large wavefunctions, making this problem computationally intractable for large and strongly-correlated systems [1]. In contrast, gate-based quantum computing presents a promising solution, offering the potential to represent electronic wavefunctions with polynomially scaling resources using quantum algorithms for the simulation of chemical systems [2]. In other words, quantum computers are a natural tool of choice for simulating processes that are inherently quantum [3].

In the last two decades, many advancements in quantum computing have been made in both hardware and software, bringing us closer to being able to simulate molecular systems. Despite these advancements, we remain in the so-called Noisy Intermediate Scale Quantum (NISQ) era [4], characterised by challenges such as poor qubit fidelity, low qubit connectivity and limited coherence times [5]. The NISQ era represents a transitional phase in quantum computing, where quantum devices are not yet error-corrected but are still capable of performing computations beyond the reach of classical computers. Overcoming the limitations of the NISQ era is crucial for realising the full potential of quantum computing in various fields, including quantum chemistry and materials science.

In this thesis, we focus on the Unitary Coupled Cluster (UCC) ansatz [6], imple-

mented on quantum devices using the Variational Quantum Eigensolver (VQE) algorithm [7]. In particular, we are concerned with the study of the excitation operators used to prepare UCC ansätze representing fermionic wavefunctions. The VQE algorithm is a method used to estimate the ground state energy of a molecular Hamiltonian by preparing a trial wavefunction, calculating its energy expectation value on a quantum device, then optimising the wavefunction parameters classically until the energy converges to the best approximation for the ground state energy [8]. It is recognised as a leading algorithm for quantum simulation on NISQ devices due to its reduced resource requirements in terms of qubit count and coherence time [9].

We build on the work of Yeung [3] on Pauli gadgets, Yordanov *et al* [10] on fermionic excitation operators and Cowtwan *et al* [11], concerning ourselves with two main questions: can we use the ZX calculus to gain insights into the structure of the UCC ansatz in the context of VQE algorithms for quantum chemistry? Secondly, in the context of NISQ devices, can we use these insights to build better ansätze with reduced circuit depth and more efficient resources? By attempting to reduce circuit depth, we are addressing the major source of error present in NISQ devices – the noise of today’s quantum hardware [11].

- **Chapter 1** develops the mathematical foundation for simulating molecules on quantum computers.
- **Chapter 2** introduces the generators of the ZX calculus and its rewrite rules.
- **Chapter 3** introduces Pauli gadgets, the basic building blocks of fermionic ansätze, and their interaction with other quantum gates.
- **Chapter 4** explores controlled rotations in terms of phase polynomials.
- **Chapter 5** applies the theory developed thus far to show how excitation operators can be expressed in terms of controlled rotations in the ZX calculus.
- **Chapter 6** introduces the software package ZxFermion that we built, demonstrating how it can be used to replicate the research done in this thesis.

Contents

1	Background	1
1.1	Context & Motivation	2
1.2	Electronic Structure Theory	4
1.3	Unitary Coupled Cluster Ansatz	9
1.4	Variational Quantum Eigensolver	10
2	ZX Calculus	11
2.1	Generators	12
2.2	Rewrite Rules	16
3	Pauli Gadgets	18
3.1	Phase Gadgets	19
3.2	Pauli Gadgets	22
3.3	Commutation Relations	23
4	Controlled Rotations	26
4.1	Singly Controlled-Rotations	27
4.2	Higher Order Controlled-Rotations	29
5	Excitation Operators	31
5.1	One Body Excitation Operators	32
5.2	Two Body Excitation Operators	35

Contents

6	ZxFermion Software	37
6.1	Creating Gadgets and Circuits	38
6.2	Manipulating Circuits	39
7	Conclusion	41
7.1	Summary	41
7.2	Future Work	41
Appendices		
Bibliography		45

Chapter 1

Background

1. Background

1.1 Context & Motivation

The Variational Quantum Eigensolver (VQE) is a promising hybrid quantum-classical algorithm for achieving quantum advantage on NISQ devices [12]. Developed in 2014 by Peruzzo and McClean *et al* [13], the VQE algorithm divides the problem of estimating the ground-state energy of a molecule into two parts – computing the energy of a state on a quantum device, then classically optimising the state until it converges to a good estimate of the ground state. One advantage of the VQE algorithm is its ability to adapt to different hardware requirements [8].

VQE algorithms implement fermionic states on quantum devices via the unitary coupled cluster method [14]. By preparing quantum states as a sequence of unitary excitation operations acting on some reference state, we define the unitary product state (UPS) ansatz [15], allowing us to parametrically explore the Hilbert space of possible quantum states [8].

The Discretely and Continuously Optimized Variational Quantum Eigensolver (DISCO-VQE) is a specific type of VQE developed by Burton *et al.* [15]. This algorithm generates multiple ansätze, each corresponding to a unique UPS wavefunction, but yielding the same energy expectation value. This means that different sequences of unitary excitation operators are employed to rotate the reference state to a state approximating the true ground state. This approach suggests an equivalence in capturing the correlation characteristics observed in the ground state.

In this context, our research focuses on the diagrammatic representation of unitary excitation operators in the ZX calculus, a diagrammatic language for reasoning about quantum processes [16]. Our initial goal was to identify a generalised structure for these excitation operators within the ZX calculus, anticipating that by doing so, we might discover a way of demonstrating the equivalence of different VQE outputs with the same energy expectation value. Through this, we aimed to uncover novel methods for optimizing ansätze that represent fermionic wavefunctions. Additionally, by developing a representation for these excitation operators that is independent

1. Background

of specific architectural constraints, we sought to gain deeper insights into the structure of UPS ansätze and the nature of correlations in molecular quantum systems. This broader understanding could potentially lead to more efficient and effective quantum simulations.

This eventually led us to the work done by Yordanov *et al* [10], which shows that excitation operators can be re-expressed in terms of controlled rotations. Throughout the course of our research, we were able to demonstrate diagrammatically the correspondence between these excitation operators and controlled rotations. Consequently, a significant portion of this thesis revolves around developing the diagrammatic techniques essential for replicating the findings of Yordanov *et al* in the ZX calculus.

In addition to our research goals, this thesis aims to introduce the ZX calculus in the context of quantum chemistry. While quantum chemistry is anticipated to be a principal application of quantum computing, it remains an area with limited engagement among Master’s level researchers in Chemistry. Therefore, we hope that this thesis, along with the tools developed herein, will help lower the barrier to entry for future Master’s students interested in quantum computing. By providing a solid foundation and practical insights, we aim to facilitate a smoother transition and foster greater interest in this rapidly developing field.

To summarise our research objectives,

1. Use the ZX calculus to gain insights into the structure of UPS ansätze and the nature of correlations in molecular quantum systems.
2. Utilise these insights to rationalise the different outputs of VQE algorithms that yield the same energy.
3. Identify a general representation of excitation operators within the ZX calculus that is independent of specific architectural constraints.
4. Leverage this general representation to discover more efficient implementations of fermionic ansätze in terms of quantum resources.

1. Background

1.2 Electronic Structure Theory

Electronic Structure Problem

The main interest of electronic structure theory is finding approximate solutions to the eigenvalue equation of the full molecular Hamiltonian. Specifically, we seek solutions to the non-relativistic time-independent Schrödinger equation.

$$H = -\sum_{i=1}^N \frac{1}{2} \nabla_i^2 - \sum_{i=1}^M \frac{1}{2M_i} \nabla_i^2 - \sum_{i=1}^N \sum_{j=1}^M \frac{Z_j}{|r_i - R_j|} + \sum_{i=1}^N \sum_{j>i}^N \frac{1}{|r_i - r_j|} + \sum_{i=1}^M \sum_{j>i}^M \frac{Z_i Z_j}{|R_i - R_j|}$$

Figure 1.1: Full molecular Hamiltonian in atomic units, where Z_i is the charge of nucleus i and M_i is its mass relative to the mass of an electron.

The full molecular Hamiltonian, H , describes all of the interactions within a system of N interacting electrons and M nuclei. The first term corresponds to the kinetic energy of all electrons in the system. The second term corresponds to the total kinetic energy of all nuclei. The third term corresponds to the pairwise attractive Coulombic interactions between the N electrons and M nuclei, whilst the fourth and fifth terms correspond to all repulsive Coulombic interactions between electrons and nuclei respectively.

We are able to simplify the problem to an electronic one using the Born-Oppenheimer approximation. Motivated by the large difference in mass of electrons and nuclei, we can approximate nuclei as stationary on the timescale of electronic motion such that the electronic wavefunction depends only parametrically on the nuclear coordinates. Within this approximation, the nuclear kinetic energy term can be neglected and the nuclear repulsive term is considered to be constant. The resulting equation is the electronic Hamiltonian for N electrons.

$$H = -\sum_{i=1}^N \frac{1}{2} \nabla_i^2 - \sum_{i=1}^N \sum_{j=1}^M \frac{Z_j}{|r_i - R_j|} + \sum_{i=1}^N \sum_{j>i}^N \frac{1}{|r_i - r_j|}$$

Figure 1.2: Electronic molecular Hamiltonian in atomic units.

Throughout the remainder of this text, we will concern ourselves only with the

1. Background

electronic Hamiltonian, simply referring to it as the Hamiltonian, H . The solution to the eigenvalue equation involving the electronic Hamiltonian is the electronic wavefunction, which depends only parametrically on the nuclear coordinates. It is solved for fixed nuclear coordinates, such that different arrangements of nuclei yields different functions of the electronic coordinates. The total molecular energy can then be calculated by solving the electronic Schrödinger equation and including the constant repulsive nuclear term.

Many-Electron Wavefunctions

The many-electron wavefunction, which describes all fermions in given molecular system, must satisfy the Pauli principle. This is an independent postulate of quantum mechanics that requires the many-electron wavefunction to be antisymmetric with respect to the exchange of any two fermions.

A spatial molecular orbital is defined as a one-particle function of the position vector, spanning the whole molecule. The spatial orbitals form an orthonormal set $\{\psi_i(\mathbf{r})\}$, which if complete can be used to expand any arbitrary single-particle molecular wavefunction, that is, an arbitrary single-particle function of the position vector. In practice, only a finite set of such orbitals is available to us, spanning only a subspace of the complete space. Hence, wavefunctions expanded using this finite set are described as being ‘exact’ only within the subspace that they span.

We will now introduce the spin orbitals $\{\phi_i(\mathbf{x})\}$, that is, the set of functions of the composite coordinate \mathbf{x} , which describes both the spin and spatial distribution of an electron. Given a set of K spatial orbitals, we can construct $2K$ spin orbitals by taking their product with the orthonormal spin functions $\alpha(\omega)$ and $\beta(\omega)$. Whilst the Hamiltonian operator makes no reference to spin, it is a necessary component when constructing many-electron wavefunctions in order to correctly antisymmetrise the wavefunction with respect to fermion exchange. Constructing the antisymmetric many-electron wavefunction from a finite set of spin orbitals amounts to taking the appropriate linear combinations of symmetric products of N spin orbitals.

1. Background

A general procedure for this is achieved by constructing a Slater determinant from the finite set of spin orbitals, where each row relates to the electron coordinate \mathbf{x}_n and each column corresponds to a particular spin orbital ϕ_i [17].

$$\psi(\mathbf{x}_1, \mathbf{x}_2) = \frac{1}{\sqrt{N!}} \begin{vmatrix} \phi_i(\mathbf{x}_1) & \phi_j(\mathbf{x}_1) & \dots & \phi_k(\mathbf{x}_1) \\ \phi_i(\mathbf{x}_2) & \phi_j(\mathbf{x}_2) & \dots & \phi_k(\mathbf{x}_2) \\ \vdots & \vdots & & \vdots \\ \phi_i(\mathbf{x}_N) & \phi_j(\mathbf{x}_N) & \dots & \phi_k(\mathbf{x}_N) \end{vmatrix}$$

Figure 1.3: Slater determinant representing an antisymmetrised N -electron wavefunction.

By constructing Slater determinants and antisymmetrising the many-electron wavefunction to meet the requirements of the Pauli principle, we have incorporated exchange correlation, in that, the motion of any two electrons with parallel spins is now correlated [17].

The Hartree-Fock method yields a set of orthonormal spin orbitals, which when used to construct a single Slater determinant, gives the best variational approximation to the ground state of a system [17]. By treating electron-electron repulsion in an average way, the Hartree-Fock approximation allows us to iteratively solve the Hartree-Fock equation for spin orbitals until they become the same as the eigenfunctions of the Fock operator. This is known as the Self-Consistent Field (SCF) method and is an elegant starting point for finding approximate solutions to the many-electron wavefunction.

For an N electron system, and given a set of $2K$ Hartree-Fock spin orbitals, where $2K > N$, there exist many different single Slater determinants. The Hartree-Fock groundstate being one of these. The remainder are excited Slater determinants, recalling that all of these must be orthogonal to one-another. By treating the Hartree-Fock ground state as a reference state, we can describe the excited states relative to the reference state, as single, double, \dots , N -tuple excited states [17].

1. Background

Second Quantisation

In second quantisation, both observables and states (by acting on the vacuum state) are represented by operators, namely the creation and annihilation operators [18]. In contrast to the standard formulation of quantum mechanics, operators in second quantisation incorporate the relevant Bose or Fermi statistics each time they act on a state, circumventing the need to keep track of symmetrised or antisymmetrised products of single-particle wavefunctions [19]. Put differently, the antisymmetry of an electronic wavefunction simply follows from the algebra of the creation and annihilation operators, which greatly simplifies the discussion of systems of many identical interacting fermions [18], [19].

The Fock space is a linear abstract vector space spanned by N orthonormal occupation number vectors, each representing a single Slater determinant [18]. Hence, given a basis of N spin orbitals we can construct 2^N single Slater determinants, each corresponding to a single occupation number vector in the full Fock space. The occupation number vector for fermionic systems is succinctly denoted in Dirac notation as below, where the occupation number f_j is 1 if spin orbital j is occupied, and 0 if spin orbital j is unoccupied.

$$|\psi\rangle = |f_{n-1} f_{n-2} \dots f_1 f_0\rangle \quad \text{where } f_j \in 0, 1$$

Whilst there is a one-to-one mapping between Slater determinants with canonically ordered spin orbitals and the occupation number vectors in the Fock space, it is important to distinguish between the two since, unlike the Slater determinants, the occupation number vectors have no spatial structure and are simply vectors in an abstract vector space [18].

Operators in second quantisation are constructed from the creation and annihilation operators a_j^\dagger and a_j , where the subscripts i and j denote the spin orbital. a_j^\dagger and a_j are one another's Hermitian adjoints, and are not self-adjoint [18]. Taking the excitation of an electron from spin orbital 0 to spin orbital 1 as an example, we can

1. Background

construct the following excitation operator.

$$a_1^\dagger a_0 |0 \dots 01\rangle = |0 \dots 10\rangle$$

Due to the fermionic exchange anti-symmetry imposed by the Pauli principle, the action of the creation and annihilation operators introduces a phase to the state that depends on the parity of the spin orbitals preceding the target spin orbital.

$$\begin{aligned} a_j^\dagger |f_{n-1} \dots f_{j+1}, 0, f_{j-1} \dots f_0\rangle &= (-1)^{\sum_{s=0}^{j-1} f_s} |f_{n-1} \dots f_{j+1}, 1, f_{j-1} \dots f_0\rangle \\ a_j |f_{n-1} \dots f_{j+1}, 1, f_{j-1} \dots f_0\rangle &= (-1)^{\sum_{s=0}^{j-1} f_s} |f_{n-1} \dots f_{j+1}, 0, f_{j-1} \dots f_0\rangle \end{aligned}$$

In second quantisation, this exchange anti-symmetry requirement is accounted for by the anti-commutation relations of the creation and annihilation operators.

$$\{\hat{a}_j, \hat{a}_k\} = 0 \quad \{\hat{a}_j^\dagger, \hat{a}_k^\dagger\} = 0 \quad \{\hat{a}_j, \hat{a}_k^\dagger\} = \delta_{jk} \hat{1}$$

The phase factor required for the second quantised representation to be consistent with the first quantised representation is automatically kept track of by the anticommutation relations of the creation and annihilation operators [18].

With these creation and annihilation operators in mind, the Hamiltonian in second quantisation can be expressed as follows.

$$\hat{H} = \sum_{ij} h_{ij} a_i^\dagger a_j + \frac{1}{2} \sum_{ijkl} h_{ijkl} a_i^\dagger a_j^\dagger a_k a_l + h_{\text{Nu}}$$

Where the one-body matrix element h_{ij} corresponds to the kinetic energy of an electron and its interaction energy with the nuclei, and the two-body matrix element h_{ijkl} corresponds to the repulsive interaction between electrons i and j .

$$\begin{aligned} h_{ij} &= \int_{-\infty}^{\infty} \psi_{i(x_1)}^* \left(-\frac{1}{2} \nabla^2 + \hat{V}_{(x_1)} \right) \psi_{j(x_1)} d^3 x_1 \\ h_{ijkl} &= \int_{-\infty}^{\infty} \int_{-\infty}^{\infty} \psi_{i(x_1)}^* \psi_{j(x_2)}^* \left(\frac{1}{|x_1 - x_2|} \right) \psi_{k(x_2)} \psi_{l(x_1)} d^3 x_1 d^3 x_2 \end{aligned}$$

h_{Nu} is a constant corresponding to the repulsive interaction between nuclei. These matrix elements are computed classically, allowing us to simulate only the inherently quantum aspects of the problem on a quantum computer.

1. Background

1.3 Unitary Coupled Cluster Ansatz

As suggested by Peruzzo *et al* [13], the Unitary Coupled Cluster (UCC) formulation of a wavefunction can be efficiently implemented on a quantum computer using quantum gates. We refer to the UCC wavefunction as the UCC ansatz $|\psi(\boldsymbol{\theta})\rangle$, defining it as some unitary excitation operator $U(\boldsymbol{\theta})$ acting on a reference state.

$$|\psi(\boldsymbol{\theta})\rangle = U(\boldsymbol{\theta}) |\psi_0\rangle = e^{\hat{T}(\boldsymbol{\theta}) - \hat{T}^\dagger(\boldsymbol{\theta})} |\psi_0\rangle$$

Where $|\psi_0\rangle$ is a single reference Slater determinant, usually the Hartree-Fock groundstate obtained via the self-consistent field method. The operator $\hat{T}(\boldsymbol{\theta})$ is a linear combination of fermionic excitation operators, parametrised by coupled cluster amplitudes $\boldsymbol{\theta}$. The exponential of the anti-Hermitian linear combination, $\hat{T}(\boldsymbol{\theta}) - \hat{T}^\dagger(\boldsymbol{\theta})$, is therefore by definition, unitary.

$$\hat{T}(\boldsymbol{\theta}) - \hat{T}^\dagger(\boldsymbol{\theta}) = \sum_{i,a} \theta_i^a (a_i^\dagger a_a - a_a^\dagger a_i) + \sum_{i,j,a,b} \theta_{ij}^{ab} (a_i^\dagger a_j^\dagger a_a a_b - a_a^\dagger a_b^\dagger a_i a_j) + \dots$$

Where i, j indexes occupied spin orbitals and a, b indexes virtual, or unoccupied, spin orbitals. The resulting unitary operator $U(\boldsymbol{\theta})$ cannot be directly implemented on a quantum computer since the terms of the excitation operator do not commute. Instead, we must invoke the Trotter formula to approximate the unitary. Taking a single Trotter step $\rho = 1$, since our focus is on the NISQ setting [11], we define the UCC ansatz as the following product of k parametrised unitary operators.

$$|\psi(\boldsymbol{\theta})\rangle = \prod_{m=1}^k U_m(\theta_m) |\psi_0\rangle \quad U_m(\theta_m) = e^{\theta_m(\tau_m - \tau_m^\dagger)}$$

Where m indexes all possible excitations and $\tau_m - \tau_m^\dagger$ corresponds to our anti-Hermitian fermionic excitation operators. It has been shown by Evangelista *et al* [20] that this UCC operator can exactly parametrise any state. In practice, we truncate the possible fermionic excitations to include only single and double excitations, yielding the popular UCCSD ansatz [21].

1. Background

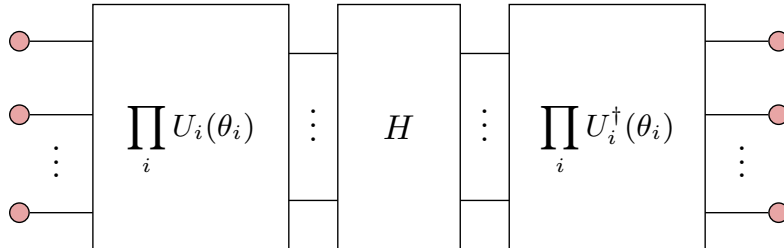
1.4 Variational Quantum Eigensolver

Parametrised quantum circuits are similar to classical neural networks in concept, but by definition of must have the same number of inputs and outputs. This requirement stems from the fact that all quantum gates must be unitary, and thus, an n qubit quantum neural network represents a $2^n \times 2^n$ unitary map [3].

The Variational Quantum Eigensolver (VQE) algorithm is a particular class of variational quantum algorithms that is used to estimate the ground state energy of molecular quantum systems. It consists of a quantum subroutine, a parametrised quantum circuit that implements some UCC ansatz representing a fermionic wavefunction, and a classical subroutine that classically optimises the UCC ansatz until it converges to the best approximation of the true ground state.

The input state for the parametrised quantum circuit is the reference state that the UCC operator $U(\boldsymbol{\theta})$ acts on, and is encoded as a pure quantum state $|\psi_0\rangle$ in the case of the single Slater determinant Hartree-Fock state. The output of the parametrised quantum circuit is an entangled state representing the UCC ansatz. That is, the the UCC ansatz $|\psi(\boldsymbol{\theta})\rangle$ represents some linear combination of vectors in the Fock space, approximating the correlation present in the true ground state.

Upon measuring the output of the parametrised quantum circuit, it collapses into a single vector in the Fock space with a probability defined by that vector's weight in the UCC ansatz. The quantum subroutine then computes the energy expectation value of the UCC ansatz using a quantum circuit consisting of the parametrised quantum circuit and the Hamiltonian for the system.



$$E(\boldsymbol{\theta}) = \langle 0 | U^\dagger(\boldsymbol{\theta}) H U(\boldsymbol{\theta}) | 0 \rangle$$

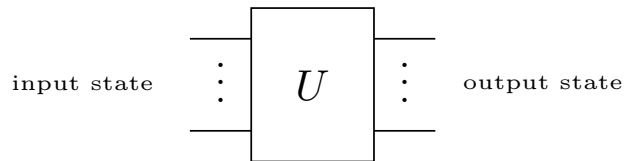
Chapter 2

ZX Calculus

In this chapter, we will introduce the ZX calculus, a diagrammatic language for reasoning about quantum processes first introduced by Coecke *et al* [16]. We will introduce the basic generators of the ZX calculus, as well as the rewrite rules that make it a language rather than just notation.

Notation

The flow of time should be interpreted from left to right. Hence, given a particular ZX diagram, we should interpret the leftmost wires as inputs, and the rightmost wires, as outputs.



This thesis uses the scalar-free ZX calculus. That is, whilst we obtain the correct operators and states, we omit their associated scalar factor. All equal signs should, therefore, be interpreted as ‘equal up to a global phase’.

Note that all of the definitions in this chapter also hold for their colour-swapped counterparts, which we have chosen to omit for brevity.

2.1 Generators

By sequentially or horizontally composing the *Z Spider* (green) and *X Spider* (red) generators, we can construct undirected multigraphs known as ZX diagrams [22]. That is, graphs that allow multiple edges between vertices. Since *only connectivity matters* in the ZX calculus, a valid ZX diagram can be arbitrarily deformed, provided that the order of inputs and outputs is preserved.

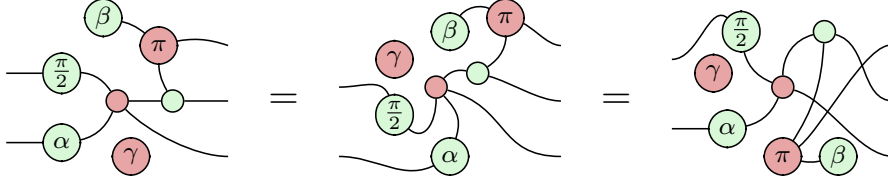


Figure 2.1: Three equivalent ZX diagrams (*only connectivity matters*).

Z Spiders (green) are defined with respect to the *Z* eigenbasis ($|0\rangle$ and $|1\rangle$) such that a Z Spider with n inputs and m outputs represents the following linear map.

$$n \begin{array}{c} \vdots \\ \text{---} \end{array} \begin{array}{c} \diagup \\ \alpha \\ \diagdown \end{array} \begin{array}{c} \vdots \\ \text{---} \end{array} m = |0\rangle^{\otimes m} \langle 0|^{\otimes n} + e^{i\alpha} |1\rangle^{\otimes m} \langle 1|^{\otimes n}$$

Figure 2.2: Interpretation of a Z Spider as a linear map.

X Spiders (red), are defined with respect to the *X* eigenbasis ($|+\rangle$ and $|-\rangle$).

$$n \begin{array}{c} \vdots \\ \text{---} \end{array} \begin{array}{c} \diagup \\ \alpha \\ \diagdown \end{array} \begin{array}{c} \vdots \\ \text{---} \end{array} m = |+\rangle^{\otimes m} \langle +|^{\otimes n} + e^{i\alpha} |-\rangle^{\otimes m} \langle -|^{\otimes n}$$

Figure 2.3: Interpretation of an X Spider as a linear map.

We can represent the *Z* eigenstates, $|0\rangle$ and $|1\rangle$, using an *X* spider with a phase of either 0 or π .

$$\text{---} \circ \text{---} = |+\rangle + |-\rangle = \sqrt{2} |0\rangle$$

Figure 2.4: $|0\rangle$ eigenstate

$$\text{---} \circ \pi \text{---} = |+\rangle - |-\rangle = \sqrt{2} |1\rangle$$

Figure 2.5: $|1\rangle$ eigenstate

2. ZX Calculus

Similarly, we can represent the X eigenstates, $|+\rangle$ and $|-\rangle$, using the corresponding Z spiders.

$$\text{---} \bigcirc \text{---} = |0\rangle + |1\rangle = \sqrt{2} |+\rangle$$

Figure 2.6: $|+\rangle$ eigenstate

$$\text{---} \bigcirc^\pi \text{---} = |0\rangle - |1\rangle = \sqrt{2} |-\rangle$$

Figure 2.7: $|-\rangle$ eigenstate

Single qubit rotations in the Z basis are represented by a Z Spider with a single input and a single output. Arbitrary rotations in the X basis are represented by the corresponding X spider. We can view these as rotations of the Bloch sphere.

$$\begin{aligned} \text{---} \bigcirc^\alpha \text{---} &= |0\rangle\langle 0| + e^{i\alpha} |1\rangle\langle 1| = \begin{pmatrix} 1 & 0 \\ 0 & e^{i\alpha} \end{pmatrix} \rightarrow \text{Bloch sphere with rotation around } z\text{-axis} \\ \text{---} \bigcirc^\alpha \text{---} &= |+\rangle\langle +| + e^{i\alpha} |-\rangle\langle -| = \frac{1}{2} \begin{pmatrix} 1 + e^{i\alpha} & 1 - e^{i\alpha} \\ 1 - e^{i\alpha} & 1 + e^{i\alpha} \end{pmatrix} \rightarrow \text{Bloch sphere with rotation around } x\text{-axis} \end{aligned}$$

We can recover the Pauli Z and Pauli X matrices by setting the angle $\alpha = \pi$.

$$\begin{aligned} \text{---} \bigcirc^\pi \text{---} &= |0\rangle\langle 0| + e^{i\pi} |1\rangle\langle 1| = \begin{pmatrix} 1 & 0 \\ 0 & -1 \end{pmatrix} \\ \text{---} \bigcirc^\pi \text{---} &= |+\rangle\langle +| + e^{i\pi} |-\rangle\langle -| = \begin{pmatrix} 0 & 1 \\ 1 & 0 \end{pmatrix} \end{aligned}$$

Figure 2.8: Pauli Z and X gates in the ZX calculus.

Composition

To calculate the matrix of a ZX diagram consisting of sequentially composed spiders, we take the matrix product. Note that the order of operation of matrix multiplication is the reverse as in the ZX diagram as we have defined it.

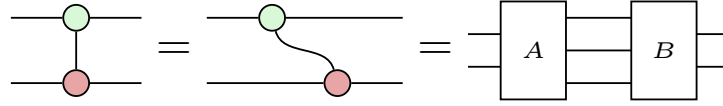
$$\text{---} \bigcirc^\alpha \text{---} \bigcirc^\beta \text{---} \bigcirc^\gamma \text{---} = \begin{pmatrix} 1 & 0 \\ 0 & e^{i\gamma} \end{pmatrix} \begin{pmatrix} 1 + e^{i\beta} & 1 - e^{i\beta} \\ 1 - e^{i\beta} & 1 + e^{i\beta} \end{pmatrix} \begin{pmatrix} 1 & 0 \\ 0 & e^{i\alpha} \end{pmatrix}$$

2. ZX Calculus

Alternatively, we could have chosen to compose the spiders in parallel, resulting in the tensor product.

$$\begin{array}{c} \textcircled{\alpha} \\ \textcircled{\beta} \end{array} = \begin{pmatrix} 1 & 0 \\ 0 & e^{i\alpha} \end{pmatrix} \otimes \begin{pmatrix} 1 + e^{i\beta} & 1 - e^{i\beta} \\ 1 - e^{i\beta} & 1 + e^{i\beta} \end{pmatrix}$$

The CNOT gate in the ZX calculus is represented by a Z spider (control qubit) and an X spider (target qubit). We can arbitrarily deform the diagram and decompose it into matrix and tensor products as follows.



We can calculate matrix A , consisting of a single-input and two-output Z Spider (4×2 matrix) and an empty wire (identity matrix), by taking the tensor product.

$$\text{Box } A \text{ with 4 wires} = \text{Diagram with 4 wires and a green circle} = \begin{pmatrix} 1 & 0 \\ 0 & 0 \\ 0 & 0 \\ 0 & 1 \end{pmatrix} \otimes \begin{pmatrix} 1 & 0 \\ 0 & 1 \end{pmatrix}$$

Similarly, to calculate the matrix B , we take the following tensor product.

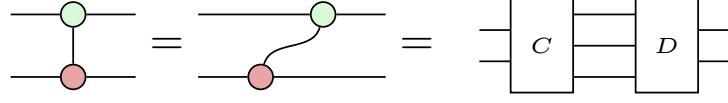
$$\text{Diagram of } B = \text{Diagram of } \text{CNOT} = \begin{pmatrix} 1 & 0 \\ 0 & 1 \end{pmatrix} \otimes \frac{1}{\sqrt{2}} \begin{pmatrix} 1 & 0 & 0 & 1 \\ 0 & 1 & 1 & 0 \end{pmatrix}$$

We can then calculate the CNOT matrix by taking the matrix product of matrix A and matrix B as follows.

$$\text{Diagram} = \left[\begin{pmatrix} 1 & 0 \\ 0 & 1 \end{pmatrix} \otimes \frac{1}{\sqrt{2}} \begin{pmatrix} 1 & 0 & 0 & 1 \\ 0 & 1 & 1 & 0 \end{pmatrix} \right] \left[\begin{pmatrix} 1 & 0 \\ 0 & 0 \\ 0 & 0 \\ 0 & 1 \end{pmatrix} \otimes \begin{pmatrix} 1 & 0 \\ 0 & 1 \end{pmatrix} \right] \simeq \begin{pmatrix} 1 & 0 & 0 & 0 \\ 0 & 1 & 0 & 0 \\ 0 & 0 & 0 & 1 \\ 0 & 0 & 1 & 0 \end{pmatrix}$$

Since *only connectivity matters* (2.1), we could have equivalently calculated the matrix of the CNOT gate by deforming the diagram as follows.

2. ZX Calculus



Had we chosen to make the first qubit the target and the second qubit the control, we would have obtained the following.

$$\text{CNOT}_{1 \rightarrow 2} = \left[\frac{1}{\sqrt{2}} \begin{pmatrix} 1 & 0 & 0 & 1 \\ 0 & 1 & 1 & 0 \end{pmatrix} \otimes \begin{pmatrix} 1 & 0 \\ 0 & 1 \end{pmatrix} \right] \left[\begin{pmatrix} 1 & 0 \\ 0 & 1 \end{pmatrix} \otimes \begin{pmatrix} 1 & 0 \\ 0 & 1 \end{pmatrix} \right] \simeq \begin{pmatrix} 1 & 0 & 0 & 0 \\ 0 & 0 & 0 & 1 \\ 0 & 0 & 1 & 0 \\ 0 & 1 & 0 & 0 \end{pmatrix}$$

Hadamard Generator

All quantum gates are unitary transformations. Therefore, up to a global phase, an arbitrary single qubit rotation U can be viewed as a rotation of the Bloch sphere about some axis. We can decompose the unitary U using Euler angles to represent the rotation as three successive rotations [22].



Figure 2.9: Arbitrary single-qubit rotation.

Recall that the Hadamard gate H switches between the $|0\rangle/|1\rangle$ and $|+\rangle/|-\rangle$ bases. That is, it corresponds to a rotation of the Bloch sphere π radians about the line bisecting the Z and X axes.

There are many equivalent ways of decomposing the Hadamard gate H using Euler angles. By choosing $\alpha = \beta = \gamma = \frac{\pi}{2}$, we obtain H up to a global phase of $\exp(-i\pi/4)$. See Appendix 7.2 for other definitions.

$$\text{Hadamard} = e^{-i\frac{\pi}{4}} \text{R}(\frac{\pi}{2}, \frac{\pi}{2}, \frac{\pi}{2}) = \frac{1}{\sqrt{2}} \begin{pmatrix} 1 & 1 \\ 1 & -1 \end{pmatrix}$$

Figure 2.10: Definition of the Hadamard generator.

2.2 Rewrite Rules

Spider Fusion

The most fundamental rule of the ZX calculus is the *spider fusion* rule [22]. It states that two spiders connected by one or more wires fuse if they are the same colour. It is the generalisation of adding the phases of successive rotations of the Bloch sphere. Since we interpret the phases α and β as $e^{i\alpha}$ and $e^{i\beta}$, it follows that the phase $\alpha + \beta$ is modulo 2π .

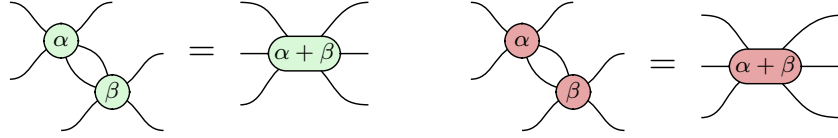
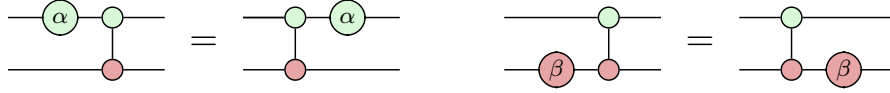


Figure 2.11: Spider fusion rule for Z spiders (left) and X spiders (right).

We can use this rule to identify commutation relations such as Z rotations commuting through CNOT controls, and X rotations, through CNOT targets.



Identity Removal

The *identity removal* rule states that any two-legged spider with no phase ($\alpha = 0$) is equivalent to a rotation by 0 radians, or identity.

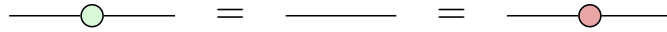
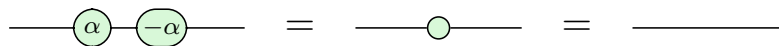


Figure 2.12: Identity removal rule.

Combining this with the spider fusion rule (2.11), we see that two successive rotations with opposite phases is equivalent to an empty wire.



Chapter 3

Pauli Gadgets

Pauli gadgets form the building blocks for ansätze for quantum chemical simulations. We will see in Chapter 5 how they can be used to construct excitation operators in UCC ansätze.

A Pauli string P is defined as a tensor product of Pauli matrices $P \in \{I, X, Y, Z\}^{\otimes n}$, where n is the number of qubits in the system. Each Pauli gate acts on a distinct qubit. Thus $Z \otimes X$ represents the Pauli Z and X gates acting on the first and second qubits respectively.

Stone's Theorem states that a strongly-continuous one parameter unitary group $U(\theta) = \exp\left(-i\frac{\theta}{2}H\right)$ is generated by the Hermitian operator H [23]. Since the Pauli matrices, and consequently Pauli strings, are Hermitian, we can use the one-to-one correspondence between Hermitian operators and one parameter unitary groups to define Pauli gadgets as the one parameter unitary groups associated with a given Pauli string.

$$\Phi_1(\theta) = \exp\left(-i\frac{\theta}{2}Z \otimes I \otimes Z\right) \quad \Phi_2(\theta) = \exp\left(-i\frac{\theta}{2}Y \otimes Z \otimes X\right)$$

3.1 Phase Gadgets

Phase gadgets are defined as the one parameter unitary groups of Pauli strings consisting of the I and Z matrices, $P \in \{I, Z\}^{\otimes n}$. They correspond to quantum circuits made of a Z rotation sandwiched between two ladders of CNOT gates.

$$= \exp \left(-i \frac{\theta}{2} Z \otimes Z \otimes Z \right)$$

Phase gadgets necessarily correspond to unitary maps which are diagonal in the Z computational basis [11], since they apply a global phase without changing the distribution of the observed state [3]. As described by Kissinger and van de Wetering [24], phase gadgets have a symmetric representation in the ZX calculus.

$$= \exp \left(-i \frac{\theta}{2} Z \otimes Z \otimes Z \right)$$

Phase gadgets can be interpreted as first copying each input in the Z basis (2.14), computing the parity of the state by taking the XOR (2.14), then multiplying the state by $\exp(-i\frac{\theta}{2})$ or $\exp(i\frac{\theta}{2})$ depending on the parity [3].

By deforming d our phase gadget in quantum circuit notation and using the identity id (2.12), spider fusion f (2.11) and bialgebra ba (2.15) rules, we are able to show the correspondence with its form in the ZX calculus.

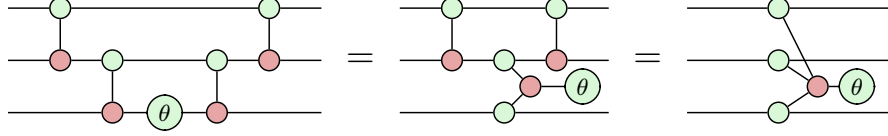
(f) $=$ (f) $=$

(d) $=$ (ba) $=$

(id) $=$ (d) $=$

3. Pauli Gadgets

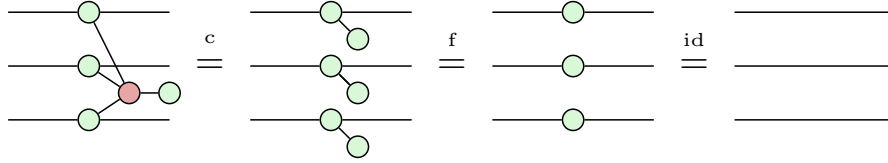
It is then a simple matter of recursively applying this proof to phase gadgets in quantum circuit notation to generalise to arbitrary arity.



As well as being intuitively self-transpose, and hence diagonal, this representation comes equipped with various rules describing the interactions of phase gadgets.

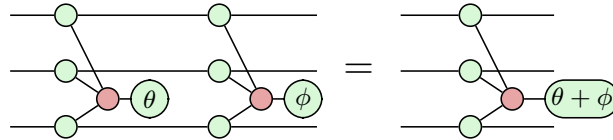
Phase Gadget Identity

Phase gadgets with an angle $\theta = 0$ can be shown to be equivalent to identity using the state copy (2.13), spider fusion (2.11) and identity removal (2.12) rules.



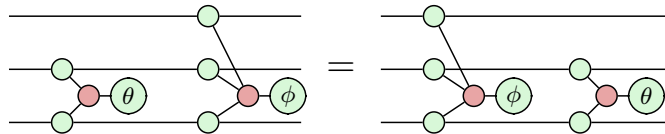
Phase Gadget Fusion

Any two adjacent phase gadgets formed from the same Pauli string fuse and their phases add. This is achieved using the spider fusion rule (2.11) and the bialgebra rule (2.15). See Appendix 7.2 for the intermediate steps.



Phase Gadget Commutation

Adjacent phase gadgets commute using the spider fusion rule (2.11).



3. Pauli Gadgets

Phase Gadget Decomposition

There are many ways of decomposing a phase gadget into quantum circuit notation. Using the bialgebra rule (2.15), we can show that a two-legged phase gadget can be decomposed in the following two ways.

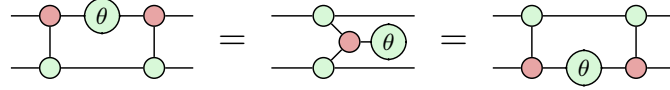
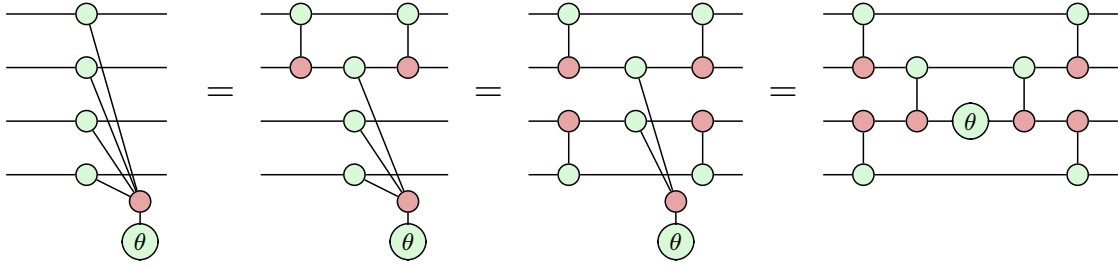
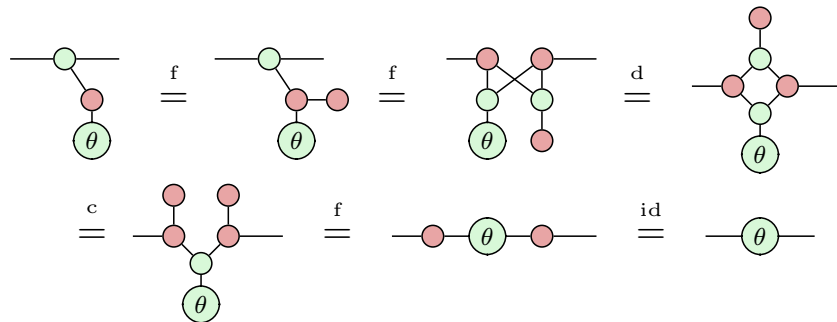


Figure 3.1: Phase gadget decomposition result.

By recursively applying this decomposition result, we can show that it is possible to decompose a phase gadget such that it has a circuit depth of $\log_2(n)$ instead of n , where n is the number of qubits.



Let us now consider a single-legged phase gadget. Using the bialgebra (2.15), spider fusion (2.11), state copy (2.13) and identity (2.12) rules, we can demonstrate its correspondence to a rotation in the Z basis.



Phase gadgets can, therefore, be thought of as the many-qubit generalisation of a rotation in the Z basis [3].

3.2 Pauli Gadgets

Pauli gadgets are defined as the one parameter unitary groups of Pauli strings consisting of all four Pauli matrices, $P \in \{I, X, Y, Z\}^{\otimes n}$ [3]. They are phase gadgets associated with a change of basis.

$$\text{Circuit with Pauli string and phase gadget} = \text{Circuit with single phase gadget} = \exp\left(-i\frac{\theta}{2}Y \otimes Z \otimes X\right)$$

Whilst phase gadgets alone cannot change the distribution of the observed state, Pauli gadgets are able to do so [3]. In chapter 5 we will see how Pauli gadgets form the building blocks in ansätze used for quantum chemical simulations.

Pauli gadgets come equipped with a similar set of rules to phase gadgets that describe their interactions with other gadgets. For instance, adjacent Pauli gadgets with *matching legs* fuse, and their phases add modulo 2π .

$$\text{Two adjacent Pauli gadgets with matching legs} = \text{Single Pauli gadget with combined phase}$$

Figure 3.2: Pauli gadget fusion rule.

Similar to the phase gadget commutation rule (3.1), we have that adjacent Pauli gadgets with *no mismatching legs* commute.

$$\text{Two Pauli gadgets with mismatching legs} = \text{Two Pauli gadgets with swapped positions}$$

Figure 3.3: Pauli gadget commutation rule.

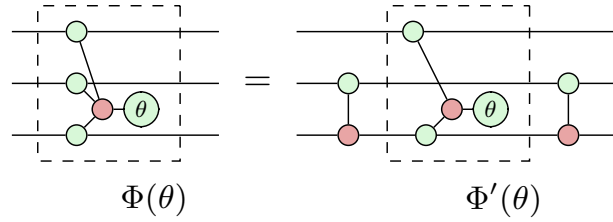
Single-legged Pauli gadgets correspond to rotations in their respective basis.

$$\text{Single-legged Pauli gadget} = \text{Rotation gate}$$

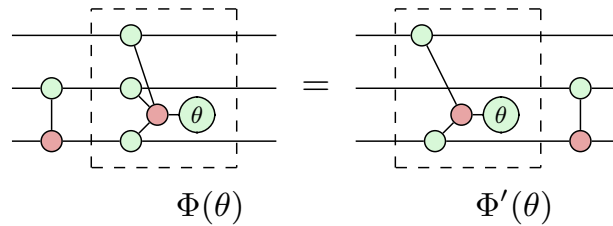
3.3 Commutation Relations

In this section we will develop a set of *commutation relations* describing the interaction of Pauli gadgets with the Clifford gates. Diagrammatically, we interpret this as ‘what happens to a Pauli gadget when a Clifford is pushed through it’.

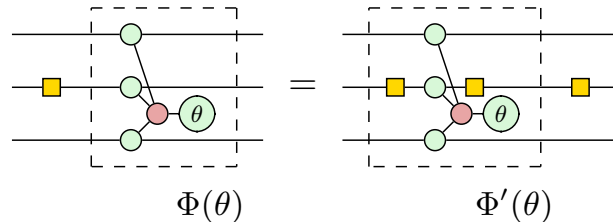
The Clifford group is the set of transformations that normalise the Pauli group. Therefore, conjugating a Pauli string P by a member of the Clifford group C is closed in the set of Pauli strings, $C^\dagger P C \in \{I, X, Y, Z\}^{\otimes n}$, where n is the number of qubits that the Clifford acts on. Similarly, conjugating a Pauli gadget $\Phi(\theta)$ by a member of the Clifford group always yields another Pauli gadget $\Phi'(\theta) = C^\dagger \Phi(\theta) C$. For instance, when $C = \text{CNOT}_{1,2}$ and $\Phi(\theta) = \exp \left[-i \frac{\theta}{2} Z \otimes Z \otimes Z \right]$, we can interpret the conjugation diagrammatically as the phase gadget decomposition result (3.1).



Recalling that the members of the Clifford group are unitary transformations, $C^{-1} = C^\dagger$, we can define *commutation relation* more formally as $\Phi(\theta)C = C\Phi'(\theta)$.



The CNOT gate is just one of many gates for which we can derive commutation relations. For example, consider the following Hadamard commutation relation.



CNOT Commutation Relations

The CNOT gate acts on two qubits ($n = 2$), therefore, we can form 16 Pauli gadgets from Pauli strings of the set of Pauli matrices, $\{I, X, Y, Z\}$ taken two at a time, with repetition. In other words, there are 16 unique commutation relations to derive to fully describe the interaction between the CNOT gate and Pauli gadgets.

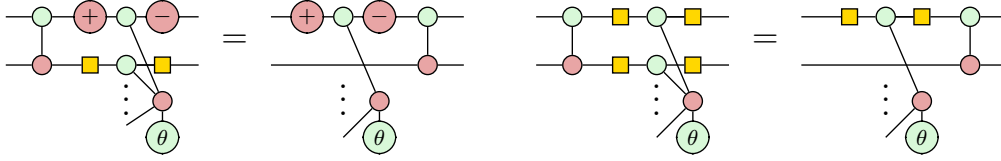
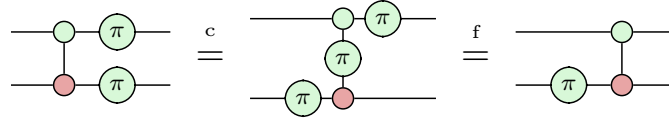


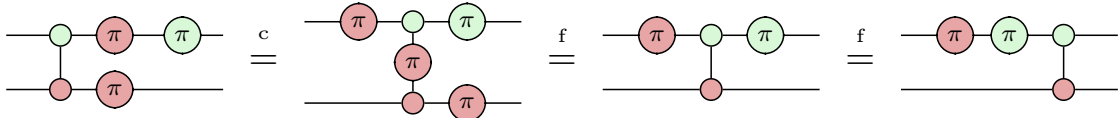
Figure 3.4: Two examples of the CNOT gate interacting with Pauli gadgets.

Whilst it is possible to derive each of these commutation relations using the Pauli gadget directly, it can be shown, through the Taylor expansion, that conjugating a Pauli gadget is equivalent to finding the one parameter unitary group of the conjugated Pauli string. Diagrammatically, this corresponds to pushing Pauli gates through some Clifford gate.

Let us illustrate the $\exp \left[-i \frac{\theta}{2} Z \otimes Z \right] \text{CNOT}_{0,1} = \text{CNOT}_{0,1} \exp \left[-i \frac{\theta}{2} I \otimes Z \right]$ commutation relation diagrammatically using the $Z \otimes Z$ Pauli string. We first push the bottom Pauli Z gate through the CNOT target using the π copy rule (2.13), then, we push the top Pauli Z gate through the CNOT control using the spider fusion rule (2.11), cancelling one of the copied Pauli Z gates in the process.



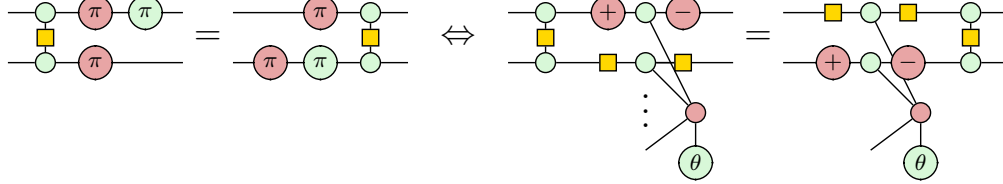
The Pauli Y gate can be expressed as a Pauli X gate followed by a Pauli Z gate, up to a global phase of $-i$ (CHECK). Below, we use this to illustrate the $\exp \left[-i \frac{\theta}{2} Y \otimes X \right] \text{CNOT}_{0,1} = \text{CNOT}_{0,1} \exp \left[-i \frac{\theta}{2} Y \otimes I \right]$ commutation relation.



3. Pauli Gadgets

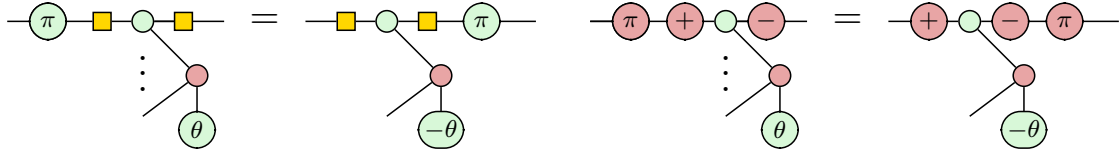
CZ Commutation Relations

Similarly, we can derive the 16 commutation relations of the CZ (controlled-Z) gate using the same method. Consider, for instance, the following example.



Pauli Commutation Relations

The Pauli matrices commute through Pauli strings by applying a global phase but leaving the Pauli string unchanged. Due to the one-to-one correspondence between Pauli strings and their corresponding Pauli gadget, we can show that the Paulis commute through Pauli gadgets by modifying their phase.



Clifford Tableaus

As pointed out by Richie Yeung, a more efficient method of identifying such commutation relations is instead to construct a Clifford tableau as in Winderl *et al* [25]. At the time, we were unaware of Clifford tableaus, however, using this method we were able to derive all 16 commutation relations (Appendix 2), demonstrating its efficacy. In Chapter 6, we choose to implement these commutation relations in our software package ZxFermion using Stim's (Clifford) `Tableau` class.

Chapter 4

Controlled Rotations

In this chapter, we will show how controlled rotations, with N controls, can be expressed as a phase polynomial consisting of 2^N phase gadgets. We will later use the results derived in this chapter to demonstrate the correspondence between excitation operators and controlled rotations in Chapter 5.

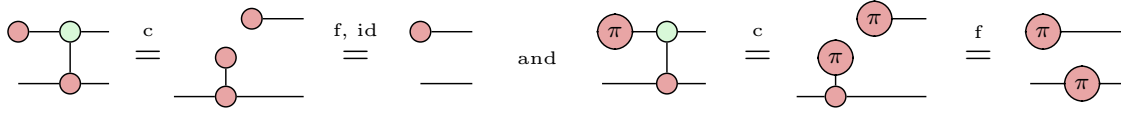
In order to replicate the results of Yordanov *et al* [10], we developed this representation of controlled rotations as phase polynomials after struggling to find related literature.

4. Controlled Rotations

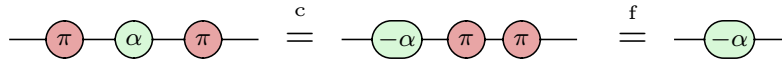
4.1 Singly Controlled-Rotations

In this section we will diagrammatically derive a singly-controlled rotation. A controlled rotation with respect to the Z eigenbasis applies a rotation to the target qubit if the control qubit is in the $|1\rangle$ state, and applies no rotation, if the control qubit is in the $|0\rangle$ state.

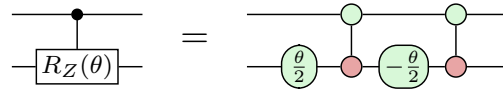
Let us start by considering the behaviour of the CNOT gate with the Z eigenstates. Using the state copy rule (2.13), we can show when the control qubit is $|0\rangle$, we obtain identity, whilst when $|1\rangle$ we obtain the Pauli X gate.



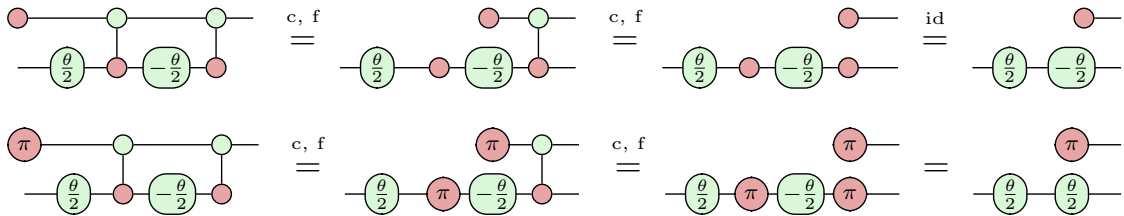
Next, using the π copy rule (2.13), we can show that conjugating a Z rotation by Pauli X gates, negates the phase of the rotation, $\alpha \rightarrow -\alpha$.



Combining these, we can construct a singly controlled rotation in the Z basis, where the black node corresponds to the control.



We can easily verify this by observing its interaction with the Z eigenstates.

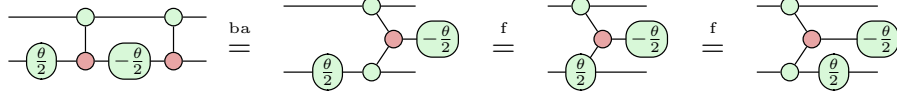


The resulting diagrams either fuse to give identity or the Pauli X gate, as expected.

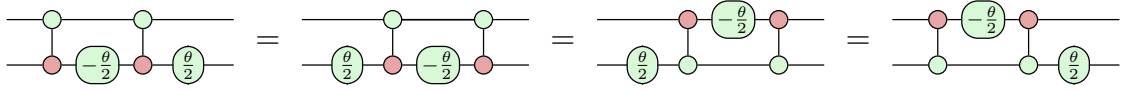


4. Controlled Rotations

Using the bialgebra rule (2.15), we can identify this structure as a two-legged phase gadget and a Z rotation, both of which commute with one another.



Using that the Z rotation commutes through the phase gadget (2.11), and the phase gadget decomposition result (3.1), we obtain four equivalent diagrams.



Deriving singly-controlled rotations in the X and Y bases amounts to conjugating the target qubit by the correct gates.

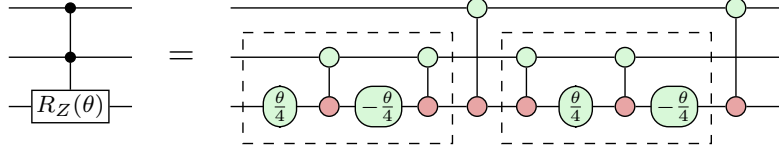


Figure 4.1: Singly-controlled X (left) and Y (right) rotations.

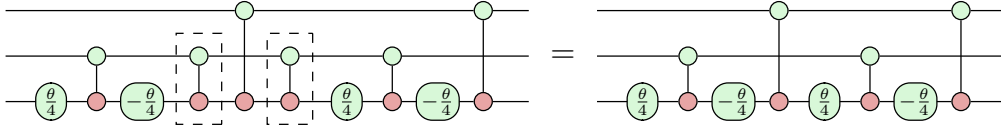
4. Controlled Rotations

4.2 Higher Order Controlled-Rotations

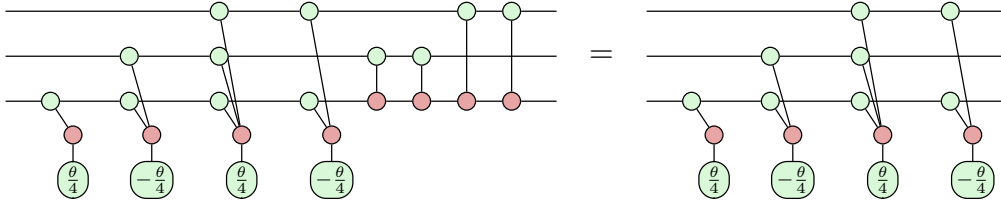
We can implement higher order controlled rotations by nesting singly-controlled rotations in CNOT gates as in Yordanov *et al* [10]. For instance, we implement a doubly-controlled Z rotation using the singly-controlled rotations highlighted.



By carefully choosing the form of the singly-controlled rotations, we can cancel the highlighted CNOT_{1,2} gates, further reducing circuit depth.



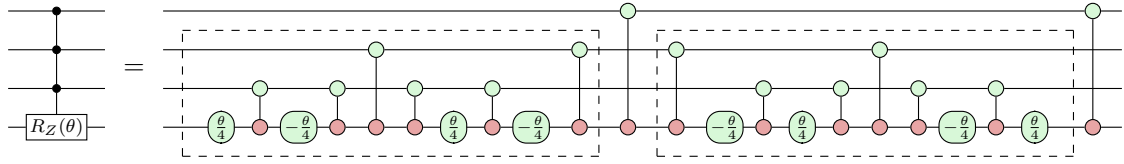
For the purposes of this thesis, we are interested in the phase polynomial that results by eliminating all CNOT gates in the circuit. We can obtain the correct phase polynomial by first expressing all Z rotations as phase gadgets, then commuting all the CNOT gates to one side of circuit, using the fact that they are self-inverse.



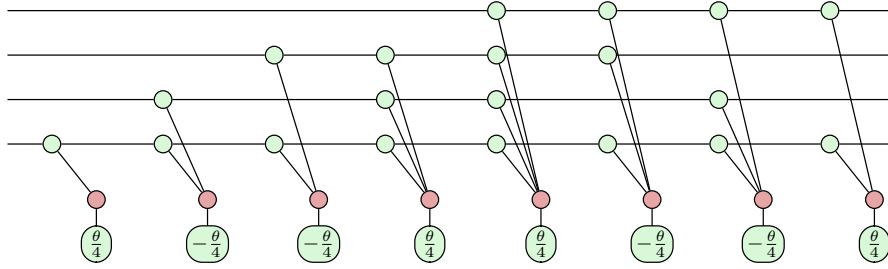
Recalling the phase gadget commutation rule, we observe that the phase polynomial that results consists only of commuting phase gadgets. Hence there are many possibly decompositions into quantum circuit notation.

By recursively applying the method of nesting controlled rotations, we can build controlled rotation of arbitrary arity. Hence, as with the doubly-controlled rotation, we can express a triply-controlled rotation by nesting two doubly-controlled rotations as follows.

4. Controlled Rotations



Using the same rules as before, we can show that a triply-controlled rotation corresponds to the following phase polynomial of commuting phase gadgets.



Chapter 5

Excitation Operators

In this chapter, we will use the theory that we have developed in Chapter 3 on Pauli gadgets and their commutation relations, and in Chapter 4 on controlled rotations, to study the excitation operators used to construct Unitary-Product State ansätze.

5. Excitation Operators

5.1 One Body Excitation Operators

Recall that a single fermionic excitation, from spin orbital p to spin orbital q , can be expressed as $a_q^\dagger a_p$ in second quantisation.

By taking a linear combination of the excitation and de-excitations acting on qubits p and q , we obtain the following anti-Hermitian fermionic one-body excitation operator.

$$\hat{\kappa}_p^q = a_q^\dagger a_p - a_p^\dagger a_q$$

Then, recalling the Jordan-Wigner transformation for the creation and annihilation operators,

$$\hat{a}_j^\dagger = \frac{1}{2}(X - iY) \otimes Z_{j-1}^\rightarrow \quad \hat{a}_j = \frac{1}{2}(X + iY) \otimes Z_{j-1}^\rightarrow$$

We can show that the anti-Hermitian fermionic one-body excitation operator can be expressed in terms of quantum gates as follows.

$$F_p^q = \frac{i}{2}(Y_p X_q - X_p Y_q) \prod_{k=p+1}^{q-1} Z_k$$

By multiplying by θ and exponentiating, we obtain the corresponding unitary *exponential one-body excitation operator*.

$$U_p^q(\theta) = \exp \left(i \frac{\theta}{2} (Y_p X_q - X_p Y_q) \prod_{k=p+1}^{q-1} Z_k \right)$$

From here onwards, we will simply refer to the unitary exponential one-body excitation operator as the *one-body excitation operator*.

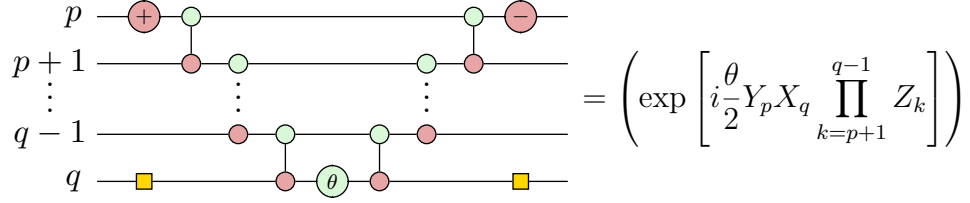
We can express this one-body excitation operator as the following commuting exponential terms.

$$U_p^q(\theta) = \exp \left(i \frac{\theta}{2} (Y_p X_q - X_p Y_q) \prod_{k=p+1}^{q-1} Z_k \right)$$

$$U_p^q(\theta) = \left(\exp \left[i \frac{\theta}{2} Y_p X_q \prod_{k=p+1}^{q-1} Z_k \right] \right) \left(\exp \left[-i \frac{\theta}{2} X_p Y_q \prod_{k=p+1}^{q-1} Z_k \right] \right)$$

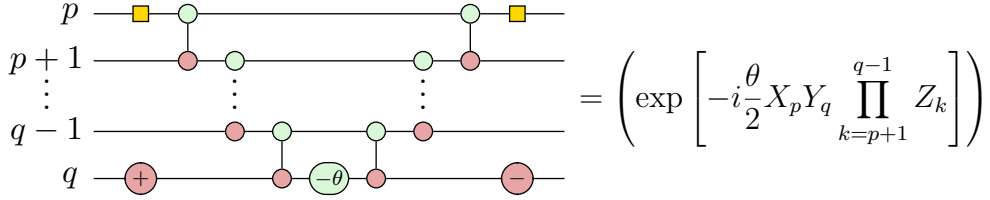
The first exponential term can be implemented by the following quantum circuit.

5. Excitation Operators



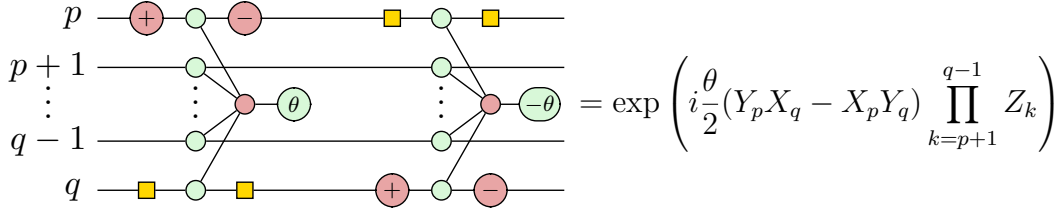
$$= \left(\exp \left[i \frac{\theta}{2} Y_p X_q \prod_{k=p+1}^{q-1} Z_k \right] \right)$$

The second exponential term can be implemented by the following circuit.



$$= \left(\exp \left[-i \frac{\theta}{2} X_p Y_q \prod_{k=p+1}^{q-1} Z_k \right] \right)$$

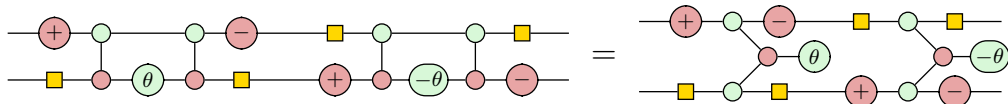
The left CNOT ladder can be thought of as calculating the parity of the fermionic state, whilst the right CNOT ladder construction uncomputes the parity. A phase of θ is then applied depending on the parity of the state. By sequentially composing (2.1) these circuits, that is, taking their matrix product, we have implemented the one-body excitation operator between qubits p and q . Expressing this operator as two Pauli gadgets, we obtain the following.



$$= \exp \left(i \frac{\theta}{2} (Y_p X_q - X_p Y_q) \prod_{k=p+1}^{q-1} Z_k \right)$$

One-Body Excitation Operators as Controlled Rotations

In this section, we will extend the work done by Yordanov *et al* [10], looking at how excitation operators can be expressed in terms of a controlled rotation. To the knowledge of the author, this work has not yet been done in the ZX calculus. Taking $U_0^1(\theta)$, $p = 0$ and $q = 1$ as an example, we have the following.

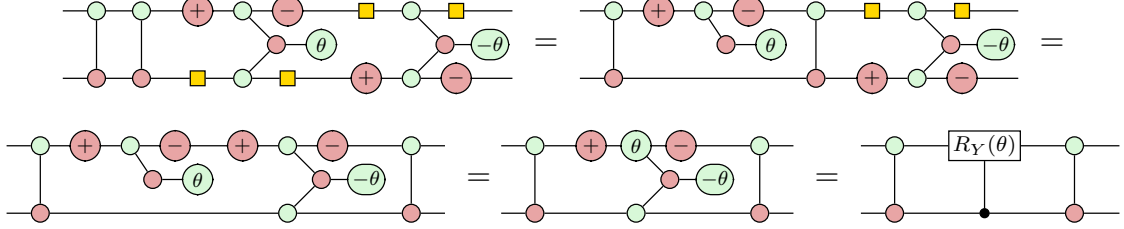


$$=$$

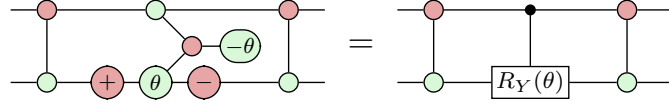
By inserting two adjacent $\text{CNOT}_{0,1}$ gates (self-inverse) into the circuit and using

5. Excitation Operators

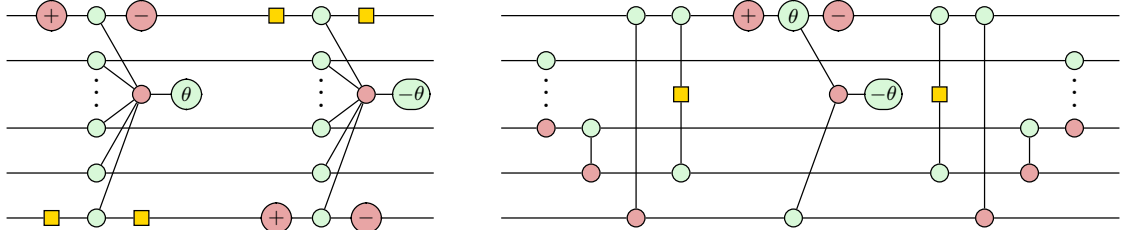
the CNOT commutation rules derived in Chapter 3, we are able to show that the one-body excitation operator can be expressed in terms of a singly-controlled rotation in the Y basis.



Had we instead chosen to insert two $\text{CNOT}_{1,0}$ gates, we would have obtained the following controlled rotation, with the control on qubit 1.



Let us now look at the general case. Yordanov *et al* [10] show that a one-body excitation operator can be expressed as a controlled rotation in the Y basis. See Appendix 7.2 for the intermediate steps.



5. Excitation Operators

5.2 Two Body Excitation Operators

A double fermionic excitation, from spin orbitals p and q to spin orbitals r and s , can be expressed as $a_r^\dagger a_s^\dagger a_q a_p$ in second quantisation.

By taking a linear combination of the excitation and de-excitation operators acting on qubits p, q, r and s , we obtain the following anti-Hermitian fermionic two-body excitation operator.

$$\hat{\kappa}_{pq}^{rs} = a_r^\dagger a_s^\dagger a_q a_p - a_p^\dagger a_q^\dagger a_s a_r$$

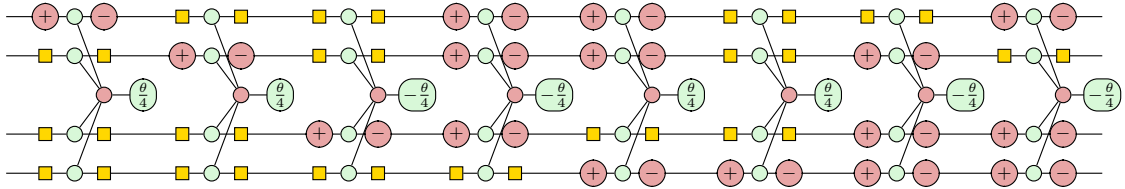
Which after applying the Jordan-Wigner transformation can be expressed in terms of the Pauli matrices as follows.

$$F_{pq}^{rs} = \frac{i}{8} (X_p X_q Y_s X_r + Y_p X_q Y_s Y_r + X_p Y_q Y_s Y_r + X_p X_q X_s Y_r - \\ Y_p X_q X_s X_r - X_p Y_q X_s X_r - Y_p Y_q Y_s X_r - Y_p Y_q X_s Y_r) \prod_{k=p+1}^{q-1} Z_k \prod_{l=r+1}^{s-1} Z_l$$

Multiplying by θ and exponentiating, we obtain the following unitary exponential two-body excitation operator, which we will refer to simply as a *two-body excitation operator*.

$$U_{pq}^{rs}(\theta) = \exp \left(i \frac{\theta}{8} (X_p X_q Y_s X_r + \dots - Y_p Y_q Y_s X_r - Y_p Y_q X_s Y_r) \prod_{k=p+1}^{q-1} Z_k \prod_{l=r+1}^{s-1} Z_l \right)$$

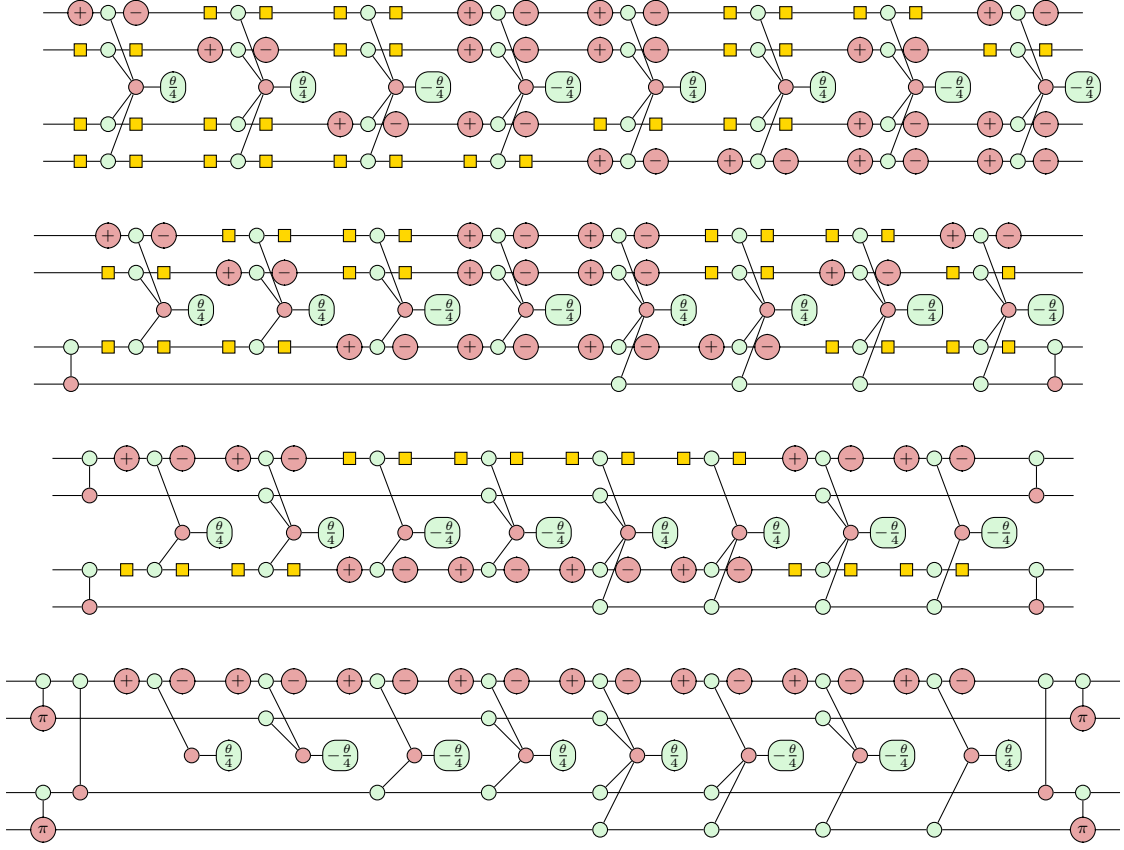
The full two-body excitation operator can be split into eight commuting exponential terms, implemented by eight Pauli gadgets. Taking $p = 0, q = 1, r = 2$ and $s = 3$ as an example, we obtain the following in Pauli gadget form.



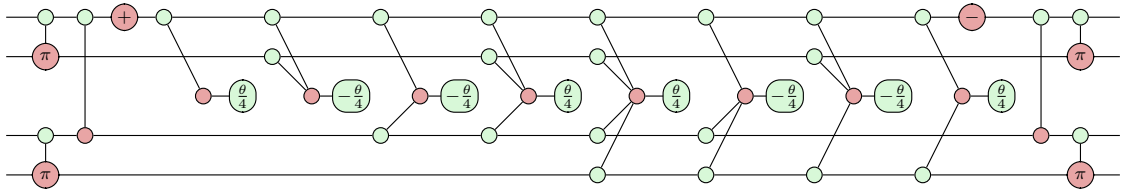
Two-Body Excitation Operators as Controlled Rotations

Using the commutation relations derived in Chapter 3, we can see that by conjugating the circuit with CNOT gates we obtain the following phase polynomial.

5. Excitation Operators



By cancelling adjacent change of basis gates, we can show that a two-body excitation operator corresponds to a triply-controlled rotation in the Y basis (recalling the result for triply controlled rotations in Chapter 4), as in Yordanov *et al.*



Chapter 6

ZxFermion Software

ZxFermion (visit github.com/aymannel/zxfermion for documentation) is a Python package that I wrote for the manipulation and visualisation of circuits of Pauli gadgets. It is built on top of the PyZX `BaseGraph` API [26] and Stim [27]. The motivation for building this package came from the need for a user-friendly tool to explore research ideas related to circuits of Pauli gadgets.

Whilst there are existing software solutions like PauliOpt, which focus on circuit simplification using architecture-aware synthesis algorithms [28], ZxFermion provides a more accessible alternative, as well as offering tools for studying the interaction of Pauli gadgets with Clifford and Pauli gates using Stim’s `Tableau` class.

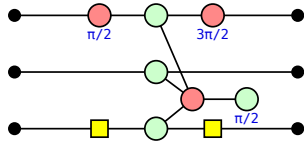
ZxFermion is designed to integrate with Jupyter notebook environments, enabling users to visualise interactive ZX diagrams directly in the output cell. The package has also undergone thorough testing, ensuring its reliability and ease of use.

All of the proofs so far derived can be replicated using ZxFermion, showcasing a noteworthy acceleration in research pace. We anticipate that both chemists and computer scientists exploring quantum computing within the VQE framework will find this software tool advantageous.

6.1 Creating Gadgets and Circuits

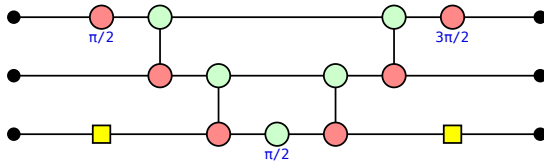
In this section, we will introduce the `Gadget` class, which we use to represent Pauli gadgets. We provide a Pauli string and a phase to instantiate a `Gadget()` object.

```
gadget = Gadget('YZX', phase=1/2)
gadget.draw()
```



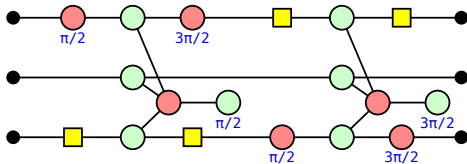
By setting the `as_gadget` option to `False`, we can view the gadget in its expanded form, that is, in quantum circuit notation.

```
gadget = Gadget('YZX', phase=1/2, as_gadget=False)
gadget.draw()
```



We can construct a circuit of Pauli gadgets using the `GadgetCircuit` class. The underlying data structure for this class is simply an ordered list.

```
gadget1 = Gadget('YZX', phase=1/2)
gadget2 = Gadget('XZY', phase=3/2)
circuit = GadgetCircuit([gadget1, gadget2])
circuit.draw()
```

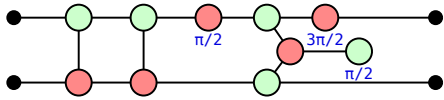


ZxFermion also implements standard quantum gates via the `CX`, `CZ`, `X`, `Z`, `XPlus`, `XMinus`, `ZPlus` and `ZMinus` classes. As we will see in the next section, we have implemented the logic describing the interaction of Pauli gadgets with these gates.

6.2 Manipulating Circuits

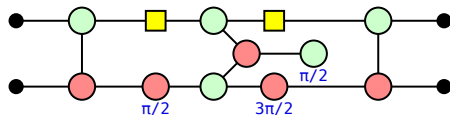
The `GadgetCircuit` class comes equipped with the `apply()` method that allows us to insert a quantum gate, and its Hermitian conjugate, into the circuit. This operation preserves the matrix corresponding to a given circuit. The method takes the quantum gate to apply as its first parameter, whilst the `start` and `end` parameters designate the insertion positions.

```
gadget = Gadget('YZ', phase=1/2)
circuit = GadgetCircuit([gadget])
circuit.apply(CX(0, 1), start=0, end=0, draw=True)
```



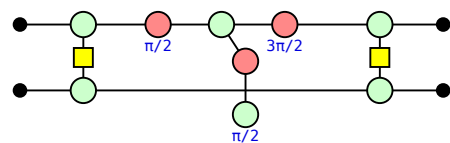
If no specific positions are specified, the insertion defaults to placing one quantum gate at the start, and its Hermitian conjugate at the end, of the circuit. The `GadgetCircuit` class then manages the relevant commutation relations, ensuring the expected gadget outcome. Hence, we below, we observe the gadget that results upon pushing a CNOT gate through the `Gadget("YZ", phase=1/2)` object.

```
circuit.apply(CX(0, 1), draw=True)
```



We could have chosen any Pauli gadget by simply instantiating the relevant `Gadget()` object. Alternatively, we could have chosen to insert any Hermitian conjugate pair of gates. The commutation logic implements Stim's `Tableau` class to identify the behaviour of a Pauli string with a given Clifford or Pauli gate.

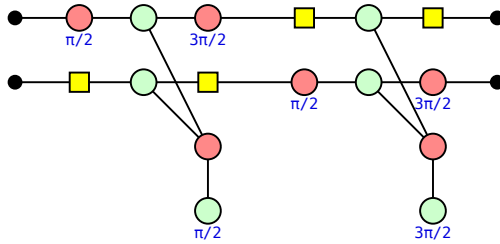
```
circuit.apply(CZ(0, 1), draw=True)
```



6. ZxFermion Software

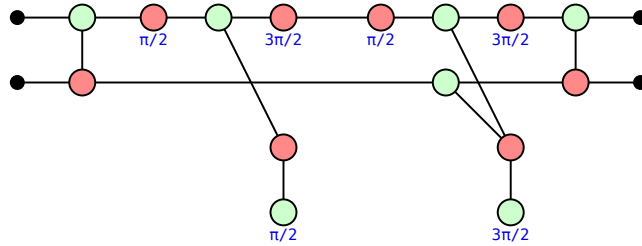
The `GadgetCircuit` class offers the ability to manipulate circuits containing multiple gadgets simultaneously. Below, we instantiate the parametrised exponential of the single excitation operator, $a_0^\dagger a_1 - a_1^\dagger a_0$, in terms of quantum gates.

```
gadget1 = Gadget('YX', phase=1/2)
gadget2 = Gadget('XY', phase=3/2)
circuit = GadgetCircuit([gadget1, gadget2])
circuit.draw()
```



Conjugating the circuit with CNOTs reveals two Pauli gadgets, that combined, represent a controlled rotation in the Y basis. We have therefore faithfully replicated the result outlined in Yordanov *et al* [10].

```
cliff = CX(0, 1)
circuit.apply(cliff, draw=True)
```



We consider it a significant achievement that with just a few lines of code, a user can now faithfully replicate derivations that took us many hours.

GIVE SOME MORE EXAMPLES IN COMPACT FORM INCLUDING CONJUGATING BY XPLUS ETC

Chapter 7

Conclusion

7.1 Summary

7.2 Future Work

Appendices

Hadamard

Below are several equivalent definitions of the Hadamard generator. Note that the two rightmost definitions do not require any scalar correction.

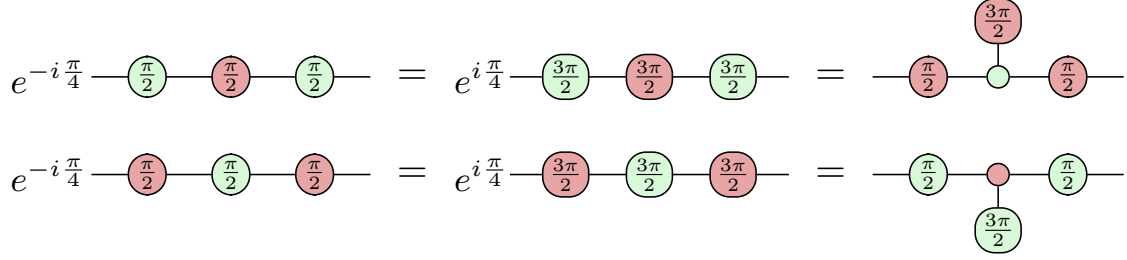
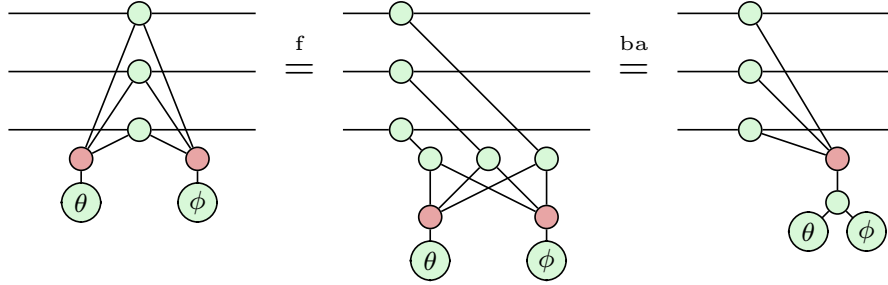


Figure 1: Equivalent definitions of the Hadamard generator.

Phase Gadgets

We can show how two adjacent phase gadgets fuse using the spider fusion (2.11) and bialgebra (2.15) rules as follows.



Clifford Conjugation Stuff

$$\begin{aligned}
 Ce^PC^\dagger &= C \sum_{n=0}^{\infty} \left(\frac{P^n}{n!} \right) C^\dagger \\
 CP^n C^\dagger &= \sum_{n=0}^{\infty} \frac{CP^n C^\dagger}{n!} \\
 CP^n C^\dagger &= \sum_{n=0}^{\infty} \frac{(CPC^\dagger)^n}{n!} \\
 CP^n C^\dagger &= (CPC^\dagger)^n
 \end{aligned}$$

CNOT Commutation Relations

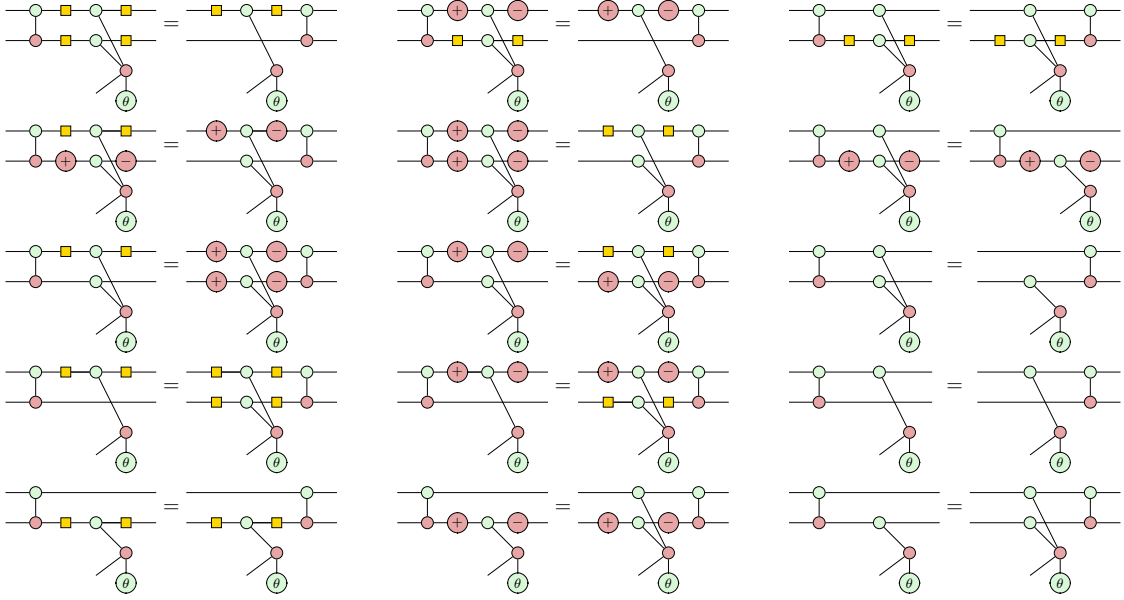
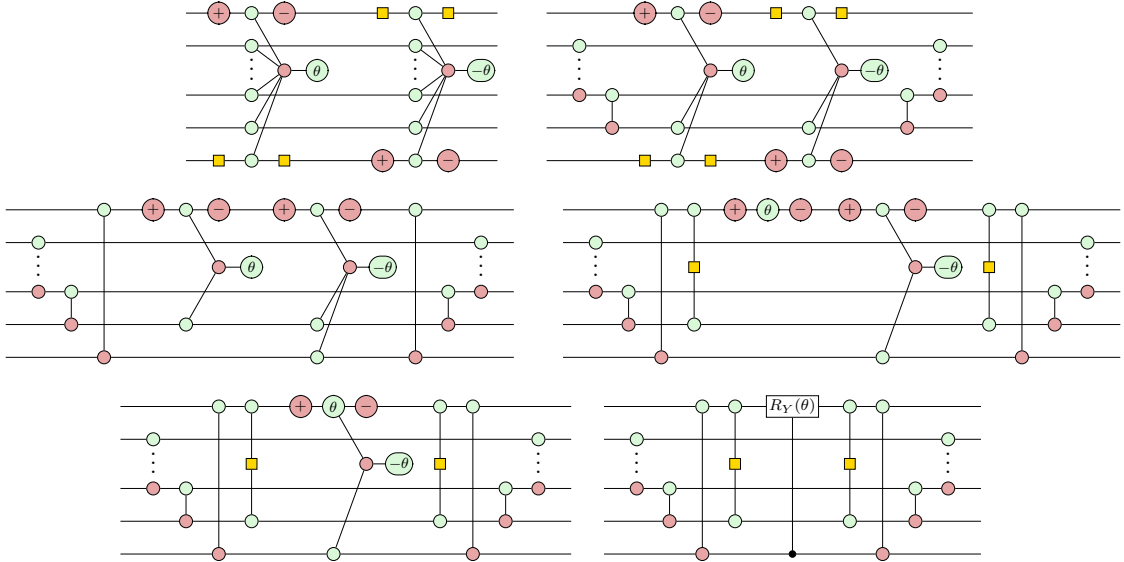


Figure 2: Complete set of CNOT commutation relations.

General One-Body Excitation Operator



Bibliography

- [1] Szalay, P. G., Müller, T., Gidofalvi, G., Lischka, H. & Shepard, R. Multi-configuration self-consistent field and multireference configuration interaction methods and applications. *Chemical Reviews* **112**, 108–181 (2011).
- [2] Kassal, I., Whitfield, J. D., Perdomo-Ortiz, A., Yung, M.-H. & Aspuru-Guzik, A. Simulating chemistry using quantum computers. *Annual Review of Physical Chemistry* **62**, 185–207 (2011).
- [3] Yeung, R. Diagrammatic design and study of ansätze for quantum machine learning (2020). 2011.11073.
- [4] Preskill, J. Quantum computing in the nisq era and beyond. *Quantum* **2**, 79 (2018).
- [5] Poulin, D. *et al.* The trotter step size required for accurate quantum simulation of quantum chemistry. *QIC 15*, 361 (2015) (2014). 1406.4920.
- [6] Romero, J. *et al.* Strategies for quantum computing molecular energies using the unitary coupled cluster ansatz. *Quantum Science and Technology* **4**, 014008 (2018).
- [7] Wecker, D., Hastings, M. B. & Troyer, M. Progress towards practical quantum variational algorithms. *Physical Review A* **92**, 042303 (2015).
- [8] McClean, J. R., Romero, J., Babbush, R. & Aspuru-Guzik, A. The theory of variational hybrid quantum-classical algorithms. *New Journal of Physics* **18**, 023023 (2016).
- [9] Kirby, W. M. & Love, P. J. Variational quantum eigensolvers for sparse hamiltonians. *Phys. Rev. Lett.* 127, 110503 (2021) **127**, 110503 (2020). 2012.07171.
- [10] Yordanov, Y. S., Arvidsson-Shukur, D. R. M. & Barnes, C. H. W. Efficient quantum circuits for quantum computational chemistry. *Physical Review A* **102**, 062612 (2020).
- [11] Cowtan, A., Simmons, W. & Duncan, R. A generic compilation strategy for the unitary coupled cluster ansatz (2020). 2007.10515.
- [12] Cerezo, M. *et al.* Variational quantum algorithms. *Nature Reviews Physics* **3**, 625–644 (2021) **3**, 625–644 (2020). 2012.09265.
- [13] Peruzzo, A. *et al.* A variational eigenvalue solver on a photonic quantum processor. *Nature Communications* **5** (2014).

Bibliography

- [14] Taube, A. G. & Bartlett, R. J. New perspectives on unitary coupled-cluster theory. *International Journal of Quantum Chemistry* **106**, 3393–3401 (2006).
- [15] Burton, H. G. A., Marti-Dafcik, D., Tew, D. P. & Wales, D. J. Exact electronic states with shallow quantum circuits from global optimisation. *npj Quantum Information* **9** (2023).
- [16] Coecke, B. & Duncan, R. Interacting quantum observables: categorical algebra and diagrammatics. *New Journal of Physics* **13**, 043016 (2011).
- [17] Szabó, A. v. & Ostlund, N. S. *Modern quantum chemistry : introduction to advanced electronic structure theory* (Mineola (N.Y.) : Dover publications, 1996). URL <http://lib.ugent.be/catalog/rug01:000906565>.
- [18] Helgaker, T., Jørgensen, P. & Olsen, J. *Molecular Electronic-Structure Theory* (Wiley, 2000).
- [19] Fetter, A. L., Walecka, J. D. & Kadanoff, L. P. *Quantum Theory of Many Particle Systems*, vol. 25 (AIP Publishing, 1972).
- [20] Evangelista, F. A., Chan, G. K.-L. & Scuseria, G. E. Exact parameterization of fermionic wave functions via unitary coupled cluster theory. *The Journal of Chemical Physics* **151** (2019). 1910.10130.
- [21] Chan, H. H. S., Fitzpatrick, N., Segarra-Martí, J., Bearpark, M. J. & Tew, D. P. Molecular excited state calculations with adaptive wavefunctions on a quantum eigensolver emulation: reducing circuit depth and separating spin states. *Physical Chemistry Chemical Physics* **23**, 26438–26450 (2021).
- [22] van de Wetering, J. Zx-calculus for the working quantum computer scientist (2020). 2012.13966.
- [23] Stone, M. H. On one-parameter unitary groups in hilbert space. *The Annals of Mathematics* **33**, 643 (1932).
- [24] Kissinger, A. & van de Wetering, J. Reducing t-count with the zx-calculus. *Phys. Rev. A* **102**, 022406 (2020) **102**, 022406 (2019). 1903.10477.
- [25] Winderl, D., Huang, Q., de Griend, A. M.-v. & Yeung, R. Architecture-aware synthesis of stabilizer circuits from clifford tableaux (2023). 2309.08972.
- [26] Kissinger, A. & van de Wetering, J. Pyzx: Large scale automated diagrammatic reasoning. *Electronic Proceedings in Theoretical Computer Science* **318**, 229–241 (2020).
- [27] Gidney, C. Stim: a fast stabilizer circuit simulator. *Quantum* **5**, 497 (2021).
- [28] Gogioso, S. & Yeung, R. Annealing optimisation of mixed zx phase circuits. *Electronic Proceedings in Theoretical Computer Science* **394**, 415–431 (2023).